Inorg. Chem. **2008**, *47*, 2113−2120

Ladders of a Magnetically Active Element in the Structure of the Novel Complex Boride $Ti_9Fe_2Ru_{18}B_8$: Synthesis, Structure, Bonding, and Magnetism

Boniface P. T. Fokwa,*,† German D. Samolyuk,‡ Gordon J. Miller,‡ and Richard Dronskowski†

Institute of Inorganic Chemistry, RWTH Aachen University, Landoltweg 1, D-52056 Aachen, Germany, and Department of Chemistry, Iowa State University, and Ames Laboratory, U.S. Department of Energy, Ames, Iowa 50011

Received October 23, 2007

Polycrystalline samples and single crystals of the complex boride $Ti_9Fe_2Ru_{18}B_8$ were synthesized by arc-melting the elements and characterized by single-crystal X-ray diffraction and energy-dispersive X-ray analysis. $Ti_9Fe_2Ru_{18}B_8$ is a new substitutional variant of the $Zn_{11}Rh_{18}B_8$ structure type, space group *P*4/*mbm* (No. 127), whose remarkable feature is that it contains one-dimensional chains of dumbbells of magnetically active Fe atoms, which form "ladders" along the *c* axis. The Fe−Fe distance within a dumbbell is 2.489(2) Å, and the Fe_2−Fe_2 distance between two dumbbells is 2.968(1) Å; in contrast, the chains are well-separated from each other by distances of at least 11.217(2) Å. According to the results of tight-binding electronic structure calculations, Ru−B and Ti−Ru contacts are responsible for the structural robustness, while Fe−Fe interactions influence the magnetic behavior. According to magnetization measurements, $Ti_9Fe_2Ru_{18}B_8$ orders ferromagnetically between 10 and 200 K. A model for ferromagnetism in this ladder-based structure identifies ferromagnetic coupling among neighboring spin-triplet Fe_2 dimers along the *c* axis as the origin of the magnetic behavior.

Introduction

Condensed matter scientists (experimentalists and theorists) have been attracted by cooperative magnetic phenomena, such as ferromagnetism, ferrimagnetism, and antiferromagnetism, for several decades.[1–3] Intermetallic magnets, in particular, are potentially very useful for systematic studies of the relationship between electronic and structural factors and magnetic properties. For example, the presence of well-separated chains of a magnetically active element in borides adopting the $Ti_3Co_5B_2$-type structure[4] has provided excellent materials for studying itinerant magnetism, in which the local magnetic moments are associated with the conduction electrons. This structure type has spawned new compounds having a wide range of magnetic properties: Pauli paramagnetism, antiferromagnetism, metamagnetism, and ferromagnetism have been observed in these compounds.[5–8] Similar chains composed of a magnetically active element have also been observed in other transition-metal borides, namely, $Zn_{10}MRh_{18}B_8$ (M = Mn, Fe, Co, Ni), whose structures are related to the aforementioned structure type; to date, their magnetic properties have not been studied.[9] Here we report the synthesis, structural characterization [based on crystal orbital Hamilton population (COHP) bonding analyses], and magnetism of a new complex boride, $Ti_9Fe_2Ru_{18}B_8$, which contains well-separated chains of iron dumbbells. Such a ladder substructure has not been previously reported for a

* To whom correspondence should be addressed. E-mail: boniface.fokwa@ac.rwth-aachen.de.
† RWTH Aachen University.
‡ Iowa State University and U.S. Department of Energy.

(1) O'Handley, R. C. *Modern Magnetic Materials*; Wiley: New York, 2000.
(2) Lueken, H. *Magnetochemie*; Teubner: Stuttgart, Germany, 1999.
(3) Chikazumi, S. *Physics of Ferromagnetism*; Clarendon Press: Oxford, U.K., 1997.
(4) Kuz'ma, Y. B.; Yarmolyuk, Y. P. *Zh. Strukt. Khim.* **1971**, *12*, 458.
(5) Nagelschmitz, E. A.; Jung, W. *Chem. Mater.* **1998**, *10*, 3189.
(6) (a) Nagelschmitz, E. A.; Jung, W.; Feiten, R.; Müller, P.; Lueken, H. *Z. Anorg. Allg. Chem.* **2001**, *627*, 523. (b) Nagelschmitz, E. A. *Dissertation*, University of Cologne, Cologne, Germany, 1995. (c) Feiten, R. *Dissertation*, RWTH Aachen University, Aachen, Germany, 1996..
(7) (a) Dronskowski, R.; Korczak, K.; Lueken, H.; Jung, W. *Angew. Chem.* **2002**, *114*, 2638. (b) Dronskowski, R.; Korczak, K.; Lueken, H.; Jung, W. *Angew. Chem., Int. Ed.* **2002**, *41*, 2528.
(8) (a) Fokwa, B. P. T.; Lueken, H.; Dronskowski, R. *Chem.—Eur. J.* **2007**, *13*, 6040. (b) Samolyuk, G. D.; Fokwa, B. P. T.; Dronskowski, R.; Miller, G. J. *Phys. Rev. B.* **2007**, *76*, 094404.
(9) Eibenstein, U.; Jung, W. *Z. Anorg. Allg. Chem.* **1998**, *624*, 802.

10.1021/ic7020963 CCC: $40.75
Published on Web 02/12/2008

magnetically active 3d element (Mn, Fe, Co, Ni) in intermetallic compounds but does occur in AFe_2S_3 (A = K, Rb, Cs).[10] Therefore, this substructure presents numerous challenges and possibilities for magnetic structure, where it is expected that short-range magnetic ordering (within each dumbbell) competes with long-range ordering (between the dumbbells).

Experimental Section

Synthesis. Polycrystalline samples and single crystals of $Ti_9Fe_2Ru_{18}B_8$ were successfully synthesized by arc-melting the elements in a water-cooled copper crucible under an argon atmosphere using a tungsten tip as a second electrode. The starting materials [titanium (chunks, 99.9%, Degussa), iron (powder, 99.9%, ABCR), ruthenium (powder, 99.9%, Umicore), and boron (crystalline pieces, 99.999%, Alfa Aesar)] were weighed in the corresponding stoichiometric ratio (total mass 0.25 g), pressed into pellets, and arc-melted under argon until homogeneous melting occurred; the argon was purified over silica gel, molecular sieves, and a titanium sponge (950 K). The products were remelted several times to ensure good homogeneity of the samples. Weight losses during the melting process were negligible. A product with a metallic luster containing several needle-shaped crystals suitable for X-ray structure analysis was obtained. The product was stable in air both as a compact bulk and as a finely ground powder.

The purity of the sample was checked by X-ray powder diffraction with Guinier powder diffraction patterns using Cu $K\alpha_1$ radiation ($\lambda = 1.54059$ Å) and silicon as an internal standard. The lattice parameters were refined on the basis of powder data using the program *WinXPOW*.[11] The presence of all of the metals and their ratios were characterized by energy-dispersive X-ray analysis (EDX) on a high-resolution, low-energy LEO 1530 SEM (Zeiss, Oberkochen, Germany) equipped with an INCA EDX system (Oxford Instruments). Averages of EDX measurements on several selected crystals provided experimental Fe:Ti and Ti:Ru ratios of 1:4.59 and 1:2.11, respectively, which agreed very well with the ratios calculated from the chemical formula $Ti_9Fe_2Ru_{18}B_8$ based on both loaded compositions and refinements of single-crystal X-ray data.

Structure Determination. A single crystal of suitable size was fixed in a glass capillary, and data were collected using a CCD single-crystal diffractometer (Bruker SMART APEX) with graphite-monochromatized Mo $K\alpha$ radiation ($\lambda = 0.71073$ Å). The X-ray intensities were corrected for absorption using a semiempirical procedure.[12] The crystal structure was refined by full-matrix least-squares refinement[13] based on F^2, using anisotropic displacement parameters for all of the metals (Ti, Fe, Ru) and isotropic ones for B. The lattice parameters obtained from the powder data were used for the single-crystal structure analysis. All relevant crystallographic data and experimental details concerning the data collection are listed in Table 1. Table 2 contains the atomic coordinates and displacement parameters, while Table 3 summarizes selected interatomic distances. Crystal structure drawings were produced using the program *Diamond*.[14] Additional details in regard to the structure determinations can be obtained from the Fachinformationszentrum Karlsruhe, D-76344 Eggenstein-Leopoldshafen, Germany, upon quoting the CSD depository number (418649).

Table 1. Crystallographic and Structure-Refinement Data for $Ti_9Fe_2Ru_{18}B_8$

formula	$Ti_9Fe_2Ru_{18}B_8$
formula weight (g/mol); $F(000)$	2448.54; 2164
crystal dimensions (mm × mm × mm)	0.15 × 0.05 × 0.04
space group; Z	*P4/mbm* (No. 127); 2
lattice parameters (Å)	$a = 17.525(3)$; $c = 2.9678(5)$
unit-cell volume (Å^3)	911.4(3)
calculated density (g/cm^3)	8.92
absorption correction	semiempirical
absorption coefficient (mm^{-1})	19.59
T_{min}; T_{max}	0.157; 0.508
diffractometer	Bruker APEX CCD, Mo Kα, graphite monochromator
θ range (deg)	$4.65 < \theta < 36.19$
hkl ranges	$-28 \le h \le 28$; $-28 \le k \le 28$; $-4 \le l \le 4$
no. of reflections; R_{int}	18824; 0.0690
no. of independent reflections	1273
no. of parameters	56
refinement method	*SHELXL*-97,[a] full matrix against F^2
R_1; wR_2 (all I)	0.0624; 0.0970
goodness of fit	1.27
diffraction peak and hole (e/Å^3)	2.957 and −3.298

[a] See ref 13.

Table 2. Atomic Coordinates and Displacement Parameters (Å^2) for $Ti_9Fe_2Ru_{18}B_8$

atom	Wyckoff position	x	y	z	U_{eq}[a]
Ru1	8*i*	0.25340(4)	0.91957(4)	0	0.0048(2)
Ru2	4*g*	0.41531(4)	0.91531(4)	0	0.0047(3)
Ru3	8*i*	0.32600(4)	0.05251(4)	0	0.0057(2)
Ru4	8*i*	0.16877(4)	0.78918(4)	0	0.0052(2)
Ru5	8*i*	0.09803(4)	0.93104(4)	0	0.0045(2)
Ti1	4*h*	0.3041(1)	0.8041(1)	1/2	0.0068(4)
Ti2	2*b*	0	0	1/2	0.0040(5)
Ti3	8*j*	0.1871(1)	0.0357(1)	1/2	0.0069(3)
Ti4	4*h*	0.3274(1)	0.1726(1)	1/2	0.0070(4)
Fe	4*h*	0.44978(8)	0.05022(8)	1/2	0.0061(4)
B1	8*j*	0.1693(6)	0.8787(6)	1/2	0.007(2)
B2	8*j*	0.3348(7)	0.9625(7)	1/2	0.010(2)

[a] U_{eq} is defined as one-third of the trace of the orthogonalized U_{ij} tensor. For boron, U_{eq} is the isotropic thermal parameter (U_{iso}).

Electronic Structure Calculations. The electronic structure calculations employed the tight-binding, linear muffin-tin orbital method with the atomic-spheres approximation (TB-LMTO-ASA)[15,16] using the Stuttgart code.[17] The exchange-correlation term was calculated within the local-spin-density approximation (LSDA), which was parametrized according to von Barth and Hedin.[18] A mesh of 54 **k** points in the irreducible wedge of the first Brillouin zone was used to obtain all integrated quantities, including density of states (DOS) and COHP[19] curves. The Wigner−Seitz radii used for these calculations were 1.43 Å (Ru1), 1.45 Å (Ru2), 1.39 Å (Ru3), 1.38 Å (Ru4, Ru5), 1.68 Å (Ti1), 1.55 Å (Ti2), 1.62 Å (Ti3), 1.73 Å (Ti4), 1.45 Å (Fe), 1.13 Å (B1 and B2).

Magnetization Measurements. Magnetic measurements were performed on polycrystalline samples (mainly selected crystals,

(10) Mitchell, R. H.; Ross, K. C.; Potter, E. G. *J. Solid State Chem.* **2004**, *177*, 1867.
(11) *WinXPOW*, version 1.06; STOE & Cie: Darmstadt, Germany, 1999.
(12) Sheldrick, G. M. *SADABS*; University of Göttingen: Göttingen, Germany, 2001.
(13) Sheldrick, G. M. *SHELXL-97, A Program for the Refinement of Crystal Structures*; University of Göttingen: Göttingen, Germany, 1997.
(14) Brandenburg, K. *DIAMOND Visual Crystal Information System*; CRYSTAL IMPACT: Bonn, Germany, 1999.
(15) Andersen, O. *Phys. Rev. B.* **1975**, *12*, 3060.
(16) Andersen, O.; Jepsen, O. *Phys. Rev. Lett.* **1984**, *53*, 2571.
(17) Krier, G.; Jepsen, O.; Burkhardt, A.; Andersen, O. K. *TB-LMTO-ASA program*, version 4.7; Max Planck Institute for Solid State Research: Stuttgart, Germany, 1995.
(18) Von Barth, U.; Hedin, L. *J. Phys. C* **1972**, *5*, 1629.
(19) Dronskowski, R.; Blöchl, P. E. *J. Phys. Chem.* **1993**, *97*, 8617.

Table 3. Selected Intersite Distances (R_{ij}) and Coordinations of the Crystallographic Sites in $Ti_9Fe_2Ru_{18}B_8$

site i	site j	R_{ij} (Å)	coordination[a]	site i	site j	R_{ij} (Å)	coordination[a]
Ru1	B2	2.192(9)	2	Ru5	Ti3	2.771(2)	2
	B1	2.211(8)	2		Ru4	2.778(1)	1
	Ru3	2.655(1)	1		Ti3	2.829(2)	2
	Ti1	2.662(2)	2		Ru5	2.968(1)	2
	Ru5	2.724(1)	1				
	Ru4	2.730(1)	1	Ti1	Ru1	2.662(2)	4
	Ti3	2.774(2)	2		Ru4	2.809(2)	4
	Ru2	2.838(1)	1		Ti1	2.968(1)	2
	Ru1	2.968(1)	2				
				Ti2	Ru5	2.572(1)	8
Ru2	B2	2.208(9)	4		Ti2	2.968(1)	2
	Ru1	2.838(1)	2				
	Fe	2.856(1)	4	Ti3	Ru5	2.771(2)	2
	Ru3	2.869(1)	2		Ru1	2.774(2)	2
	Ru2	2.968(1)	2		Ru4	2.795(2)	2
					Ru5	2.829(2)	2
Ru3	B2	2.171(9)	2		Ru3	2.866(2)	2
	Ti4	2.575(2)	2		Ti3	2.968(1)	2
	Fe	2.629(1)	2				
	Ru1	2.655(1)	1	Ti4	Ru4	2.527(2)	4
	Ti3	2.866(2)	2		Ru3	2.575(2)	4
	Ru4	2.868(1)	1		Ti4	2.968(1)	2
	Ru2	2.869(1)	1				
	Ru3	2.968(1)	2	Fe	Fe	2.489(2)	1
					Ru3	2.629(1)	4
Ru4	B1	2.159(8)	2		Ru2	2.856(1)	4
	Ti4	2.527(2)	2		Fe	2.968(1)	2
	Ru5	2.778(1)	1				
	Ti3	2.795(2)	2	B1	Ru5	2.146(8)	2
	Ti1	2.809(2)	2		Ru4	2.159(8)	2
	Ru3	2.868(1)	1		Ru1	2.211(8)	2
	Ru4	2.968(1)	2				
				B2	Ru3	2.171(9)	2
Ru5	B1	2.146(8)	2		Ru1	2.192(9)	2
	Ti2	2.572(1)	2		Ru2	2.208(9)	2

[a] Number of equivalent contacts between these two site types.

weighed portions 2–9 mg) using a SQUID magnetometer (MPMS-5S, Quantum Design, San Diego, CA) in the temperature range 4–400 K with applied fields up to 7 T. Samples were collected by manual selection of larger crystals under an optical microscope; the selected crystals were coarsely ground and encapsulated in silica tubes. Details concerning sample arrangement and measurement techniques are described elsewhere.[2] Corrections for diamagnetic and conduction-electron contributions were not applied.

Results and Discussion

Crystal Chemistry. The observed powder X-ray diffraction pattern was single-phase, and refinement of the unit cell yielded the values given in Table 1 (the lattice parameters so obtained were used for subsequent refinement of the single-crystal data). A perspective view of the structure of $Ti_9Fe_2Ru_{18}B_8$ along the [001] direction is shown in the left panel of Figure 1a. This quaternary derivative of the $Zn_{11}Rh_{18}B_8$-type structure[9] contains trigonal, tetragonal, pentagonal, and elongated hexagonal prisms of Ru atoms stacked on top of each other to form channels along the [001] direction. While the trigonal prisms are centered by boron atoms, the tetragonal and pentagonal prisms accommodate the titanium atoms, and the elongated hexagonal prisms contain dumbbells of magnetically active iron atoms. Consequently, these dumbbells are arranged in chains along the [001] direction with intrachain Fe_2-Fe_2 distances of 2.97 Å (right panel of Figure 1a), forming ladders along the *c* direction. These ladders are separated from each other by distances of at least 11.22 Å. To the best of our knowledge, similar low-dimensional structural fragments built up from a magnetically active element have not been found previously in intermetallic systems, although such ladders have been observed in AFe_2S_3 (A = K, Rb, Sr).[10] However, in these compounds, each Fe site is tetrahedrally coordinated by sulfur and shows distinct mixed valency between Fe^{2+} and Fe^{3+}.

A different low-dimensional structural fragment containing a magnetically active metal occurs in substitutional variants of borides having the $Ti_3Co_5B_2$-type structure, $M_2M'T_5B_2$ (M = Mg, Sc, Ti; M′ = Mn, Fe, Co, Ni; T = Ru, Rh).[5–8] The M′ fragments are one-dimensional chains having M′−M′ distances of 3.0 Å within a chain and 6.6 Å between chains. In fact, the $M_2M'T_5B_2$ and $Ti_9Fe_2Ru_{18}B_8$ structures are closely related to each other, as both have trigonal, tetragonal, and pentagonal prismatic arrangements of the 4d elements. The main structural difference is the presence in $Ti_9Fe_2Ru_{18}B_8$ of the elongated hexagonal prisms in which the dumbbells of the magnetically active element are located (Figure 1a). The $M_2M'T_5B_2$ compounds exhibit itinerant magnetism (antiferromagnetism, metamagnetism, and ferromagnetism) in which the type of magnetic order depends on both the identity of the magnetically active element and the number of valence electrons in the corresponding compounds.[5–8]

Other compounds that adopt the $Zn_{11}Rh_{18}B_8$-type structure and include magnetically active metal atoms are the $Zn_{10}M'Rh_{18}B_8$ series (M′ = Cr, Mn, Fe, Co, Ni). A perspective view of the structure of one of these compounds, $Zn_{10}FeRh_{18}B_8$, along the [001] direction is shown in Figure 1b. These compounds contain single-atom chains of M′ atoms having similar intrachain distances (2.8–3.0 Å) but different interchain distances (11.2 Å) compared with the $M_2M'T_5B_2$ compound series (see Figure 1b). Thus, the $M_2M'T_5B_2$ and $Zn_{10}M'Rh_{18}B_8$ cases with a common metal atom M′ are expected to have similar magnetic properties. The magnetic properties of $Ti_9Fe_2Ru_{18}B_8$, however, should differ from those of both $M_2FeT_5B_2$ and $Zn_{10}FeRh_{18}B_8$ because the local structure at the Fe sites in $Ti_9Fe_2Ru_{18}B_8$ differs from the single-atom Fe chains in the other compounds. In fact, this work reports the first example of a compound with the $Zn_{11}Rh_{18}B_8$-type structure for which a magnetic investigation has been completed.

In the $Zn_{11}Rh_{18}B_8$-type structure, iron atoms exhibit different local structures after replacing either zinc in $Zn_{11}Rh_{18}B_8$ or titanium in hypothetical "$Ti_{11}Ru_{18}B_8$". In this structure type for these two compounds, the zinc and titanium atoms occupy tetragonal, pentagonal, and elongated hexagonal prisms of rhodium or ruthenium atoms, respectively, with the elongated hexagonal prisms accommodating two-atom dumbbells. In terms of volume, one-half of the elongated hexagonal prism (i.e., the volume accommodating only one atom of the dumbbell) is smaller than a single pentagonal prism but larger than a tetragonal prism. Consequently, if atomic-size factors influence the stabilities of these compounds, substituting iron for zinc and titanium in $Zn_{11}Rh_{18}B_8$ and "$Ti_{11}Ru_{18}B_8$", respectively, should give the same result, since both zinc (atomic radius r_a = 1.31 Å) and titanium (r_a

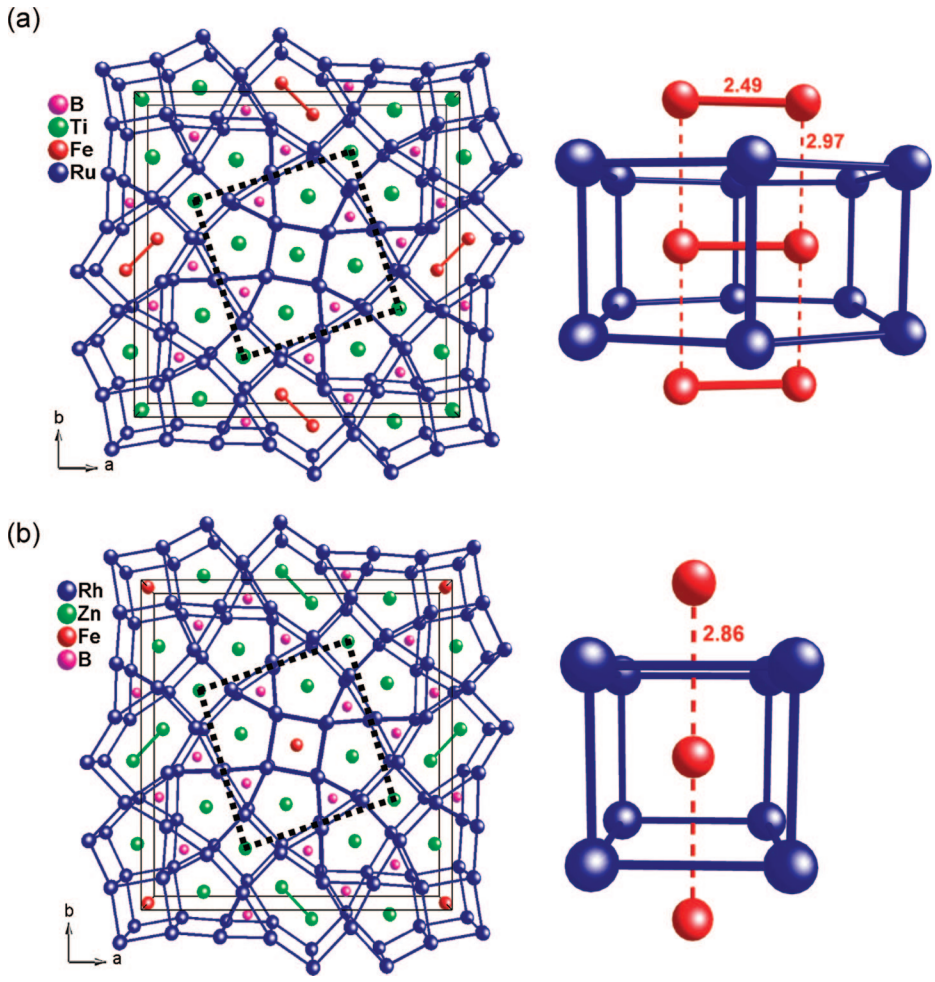

Figure 1. (a) Perspective views of (left) the crystal structure of $Ti_9Fe_2Ru_{18}B_8$ along the [001] direction and (right) an elongated hexagonal prism of Ru atoms encapsulating an Fe_2 dumbbell. (b) Perspective views of (left) the crystal structure of $Zn_{10}FeRh_{18}B_8$ along the [001] direction and (right) a tetragonal prism of Rh atoms accommodating an Fe atom. Dotted lines indicate the unit cell of the $Ti_3Co_5B_2$-type structure. Significant Fe−Fe distances (Å) are noted.

= 1.38 Å) are clearly larger than iron (r_a = 1.25 Å).[20] However, different substitution patterns emerge: in $Zn_{10}FeRh_{18}B_8$, iron replaces zinc in the smallest-volume site (the tetragonal prism), as expected from size considerations, whereas in $Ti_9Fe_2Ru_{18}B_8$, iron preferentially and unexpectedly replaces titanium in the elongated hexagonal prisms. Therefore, electronic factors as opposed to size factors should play a key role in determining the substitutional preference of titanium by iron in hypothetical "$Ti_{11}Ru_{18}B_8$", leading to $Ti_9Fe_2Ru_{18}B_8$.

Electronic Structure and Chemical Bonding. Figure 2 illustrates the total DOS curve calculated for $Ti_9Fe_2Ru_{18}B_8$ and its decomposition into contributions from the atomic constituents. The nonvanishing DOS value at the Fermi level (E_F) indicates metallic character, as expected for this intermetallic compound. The Fermi level lies 0.5 eV below a deep pseudogap in the DOS curve; states near E_F involve significant combinations of valence orbitals from all of the atomic constituents except boron. Bands located between −10 and −8 eV arise primarily from B 2s orbitals combined with Ru valence orbitals. Bands beginning near −7 eV and extending to the pseudogap at 0.5 eV above E_F involve

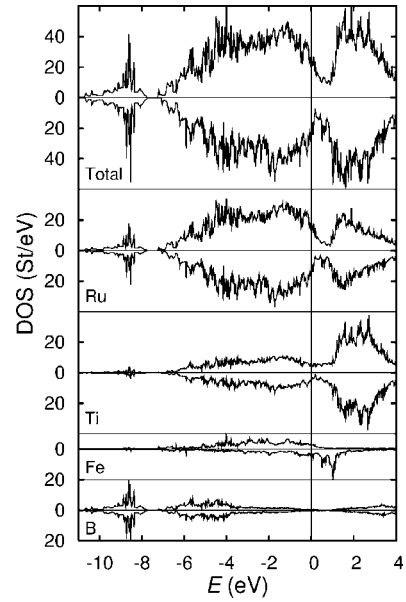

Figure 2. Total and partial DOS curves obtained from spin-polarized (LSDA) calculations for $Ti_9Fe_2Ru_{18}B_8$. The Fermi level is the energy reference.

significant combinations of B 2p, Ru 4d and 5s, and Ti 3d and 4s orbitals. Throughout this region of the total DOS

(20) Pauling, L.; Kamb, B. *Proc. Natl. Acad. Sci. U.S.A.* **1986**, *83*, 3569.

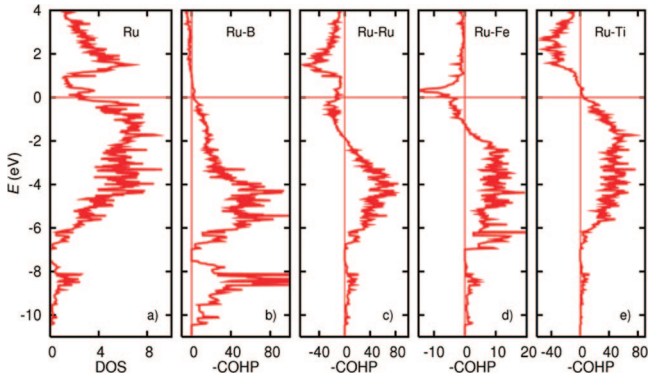

Figure 3. (a) Partial DOS of Ru atoms and COHP curves for (b) Ru−B, (c) Ru−Ru, (d) Ru−Fe, and (e) Ru−Ti contacts obtained from non-spin-polarized (LDA) calculations for $Ti_9Fe_2Ru_{18}B_8$. The Fermi level is the energy reference.

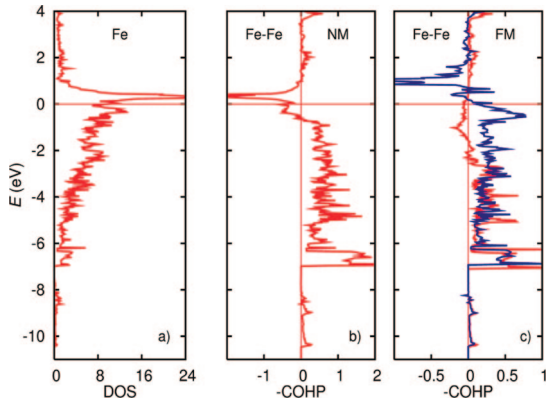

Figure 4. (a) Partial DOS of Fe atoms and COHP curves for (b) nonmagnetic (non-spin-polarized) and (c) ferromagnetic (spin-polarized) Fe−Fe bonds in $Ti_9Fe_2Ru_{18}B_8$. In (c), the red and blue curves represent the majority and minority spin bands, respectively. The Fermi level is the energy reference.

Table 4. ICOHP Values for Various Interatomic Contacts in $Ti_9Fe_2Ru_{18}B_8$, with ICOHP Values for Similar Contacts in Elemental and Binary Compounds Included for Comparison

contact	distance(s) (Å)	ICOHP (eV/bond)	related example	distance(s) (Å)	ICOHP (eV/bond)
Fe−Fe	2.49	−2.122	Fe (bcc)	2.41	−1.735
	2.97	−0.966		2.79	−0.778
Ru−B	2.15–2.21	−3.086[a]	Ru_7B_3	2.15–2.20	−2.923[a]
Ru−Ti	2.58–2.87	−1.710[a]	TiRu	2.66	−1.855
Ru−Fe	2.63–2.86	−1.310[a]	RuFe (hcp)	2.55–2.58	−1.684[a]
Ru−Ru	2.66–2.97	−0.763[a]	Ru (hcp)	2.67–2.75	−1.571[a]

[a] Average ICOHP value for a range of related interatomic distances.

curve, Ru valence orbitals dominate; the B 2p orbitals mostly contribute near the bottom of this band, whereas the Ti valence orbitals become significant closer to the Fermi level. Above the pseudogap, Ti valence orbitals make a greater contribution to the DOS; this result is similar to what is observed in the CsCl-type intermetallic compound TiRu.

The chemical bonding can be analyzed on the basis of the shapes and integrated values of the COHP curves (ICOHP = integrated value of COHP) for various interatomic interactions in the solid. These results are summarized in Figures 3 and 4 and Table 4, which for comparison also includes ICOHP values for similar interatomic interactions in related elemental and binary compounds. The COHP curves in Figure 3 indicate that Ru−B and Ru−Ti orbital interactions are optimized in $Ti_9Fe_2Ru_{18}B_8$: bonding orbitals are filled, and antibonding orbitals are empty. Both Ru−Fe and Ru−Ru contacts show antibonding character near the Fermi level. This COHP analysis suggests that it is the heteroatomic Ru−B and Ru−Ti bonds that create the structural stability of $Ti_9Fe_2Ru_{18}B_8$. In agreement with this assessment, the largest ICOHP values were found for the Ru−B and Ru−Ti contacts. The relatively short Ru−B distances, ranging from 2.15 to 2.21 Å, were slightly longer than the sum of their covalent radii (2.07 Å). Nevertheless, similar average Ru−B interatomic distances have been found in the phases Ru_2B_3 (2.18 Å),[21] $Fe_xRu_{7-x}B_3$ ($0 < x \leq 1.5$; 2.14 Å),[22] and $Ti_{1.6}Os_{1.4}RuB_2$ (2.16 Å).[23] The average ICOHP value for Ru−B bonds in $Ti_9Fe_2Ru_{18}B_8$ was 5.6% larger than that in Ru_7B_3 (see Table 4), in which the B atoms also sit in trigonal prisms. The average ICOHP value for Ru−Ti bonds also indicates significant orbital interactions, which occur in TiRu as well (see Table 4), and is reflected by the fact that the average distance (2.67 Å) was slightly shorter than the sum of the metallic radii for a coordination number (CN) of 8 (2.72 Å).[20] The average ICOHP value of the Ru−Fe contacts is smaller than that calculated for hcp-RuFe (see Table 4) but agrees with the long average Ru−Fe distance of 2.79 Å, which is 0.19 Å longer than the sum of the metallic radii for CN 12 (2.60 Å).[20] As a consequence of these significant heteroatomic interactions between Ru and the other elements, homoatomic Ru−Ru interactions are expected to be weaker than in elemental Ru because greater electron density will be engaged in Ru−X (X = B, Ti, Fe) bonds. The average ICOHP value of only −0.763 eV/Ru−Ru bond confirms this expectation, which is further supported by the wide range of Ru−Ru distances in $Ti_9Fe_2Ru_{18}B_8$, whose average of 2.87 Å is significantly longer than the ruthenium metallic distance for CN 12 (2.67 Å).[20]

Of special interest is the formation of ladders of iron atoms in this structure. The dumbbells that serve as the "rungs" of the ladders show a short Fe−Fe distance of 2.49 Å and a significant orbital interaction (ICOHP = −2.122 eV/bond). Nevertheless, the Fe−Fe COHP curve for the "nonmagnetic" (non-spin-polarized) case (Figure 4b) shows antibonding character for this bond at the Fermi level. When spin polarization is included (see Magnetism, below), the COHP curve for the minority spin electrons in this bond (blue curve in Figure 4c) shows optimized orbital interactions. The dumbbells interact with each other along the *c* axis at a distance of 2.97 Å, which is comparable to distances found in all iron-containing compounds of the $Ti_3Co_5B_2$-type structure (e.g., the $Sc_2FeRu_{5-n}Rh_nB_2$ series[8a]). Surprisingly, the corresponding ICOHP value of −0.966 eV for this long Fe−Fe bond is greater than the average ICOHP value for the Ru−Ru interactions (−0.763 eV/bond). This Fe−Fe COHP curve is also antibonding at the Fermi level. The long diagonal Fe−Fe contact between dumbbells (3.89 Å) gives an ICOHP value of only −0.041 eV/bond, suggesting that this interaction is very weak and need not be considered

(21) Lundstroem, T. *Ark. Kemi* **1969**, *30*, 115.
(22) Fokwa, B. P. T.; Dronskowski, R. *J. Alloys Compd.* **2007**, *428*, 84.
(23) Fokwa, B. P. T.; von Appen, J.; Dronskowski, R. *Chem. Commun.* **2006**, 4419.

further. Thus, $Ti_9Fe_2Ru_{18}B_8$ contains chains of Fe_2 dumbbells (i.e., a ladder substructure of iron atoms) in which a competition between short-range magnetic interactions (strong interactions within the dumbbells) and long-range ones (weaker but significant interactions between the dumbbells) should be expected.

No significant interactions for Ti−Fe, Ti−B, or Fe−B contacts in the structure were found on the basis of ICOHP values.

A qualitative rationale for the features of the total DOS curve for $Ti_9Fe_2Ru_{18}B_8$ can be obtained by analyzing the energies and numbers of the atomic orbitals (AOs) contributed by the various elements constituting this structure[24] and taking into account this COHP analysis. If we focus on just the "$Ti_9Ru_{18}B_8$" substructure, which exerts the greatest influence on structural stability, the lowest-energy AOs increase as E(B 2s) < E(Ru 4d) < E(Ti 3d) < E(B 2p). A single formula unit of $Ti_9Fe_2Ru_{18}B_8$ contains 220 valence electrons, which occupy a minimum of 110 valence orbitals. The pseudogap in the DOS curve lies slightly above this valence-electron count, so this structure requires 116.5 occupied valence orbitals (i.e., 6.5 occupied valence orbitals in excess of the minimum number required). The B 2s and Ru 4d AOs account for 98 orbitals. However, Ru atoms at the five Ru crystallographic sites in $Ti_9Fe_2Ru_{18}B_8$ experience different bonding environments: Ru atoms at the Ru1 and Ru2 sites are bonded to four B atoms in a nearly square-planar arrangement, whereas the remaining Ru sites are bonded to just two B atoms (see Tables 2 and 3). In this square-planar coordination around Ru1 and Ru2, a local Ru x^2-y^2 AO will become an Ru−B antibonding orbital and be pushed above the pseudogap. Since six atoms in the chemical formula occupy Ru1 and Ru2 sites, we can thus account for 92 occupied orbitals in this solid. The Ti 3d orbitals do not affect this number; they simply form Ti−Ru bonding combinations with the occupied Ru 4d bands. To account for the remaining occupied orbitals, we recognize that the B 2p AOs are involved in bonding interactions with the 5s and 5p AOs of Ru; of these 24 B 2p AOs, 12 contribute to Ru−B bonding orbitals and 12 contribute to Ru−B antibonding orbitals. With these 12 AOs, we now account for 104 bonding orbitals (Ru−B and Ru−Ti, on the basis of the COHP analysis). The remaining occupied orbitals originate from six of the 3d orbitals in the Fe_2 dumbbells, bringing the total to 110 occupied orbitals. In this counting strategy, we must keep in mind that the lowest-energy AOs are involved in bonding overlap with higher-energy AOs. A more detailed theoretical assessment of the electronic structure and chemical bonding of the entire class of $Zn_{11}Rh_{18}B_8$-based transition-metal borides is underway and lies outside the scope of this work.

Magnetism. In the crystal structure of $Ti_9Fe_2Ru_{18}B_8$, the presence of ladders of iron atoms reinforces the possibility of observing long-range magnetic order, which could also originate from the conduction electrons in accordance with the DOS curve for this compound. Figure 5 shows the results of magnetic measurements over the temperature range 2–400 K with applied fields (B_0) ranging up to 7 T. The presentation of the magnetic data (SI units) follows the recommendation of Hatscher et al.[25]

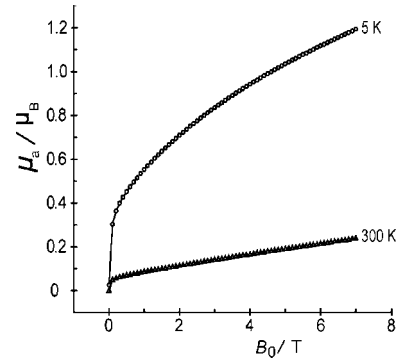

Figure 5. Magnetization as a function of applied field at 5 and 300 K for $Ti_9Fe_2Ru_{18}B_8$.

According to the variation of the atomic magnetic dipole moment (μ_a) versus applied field, at 5 K a relatively small field of 0.05 T was required in order to form a single ferromagnetic domain having an ordered moment of $0.3\mu_B$. As the applied field increased, μ_a rapidly increased, doubling in value for an applied field of 1.2 T, but remained unsaturated, reaching a value of $1.2\mu_B$ at 7 T, the highest field applied. Therefore, since there is only one iron site in the structure, $Ti_9Fe_2Ru_{18}B_8$ is a ferromagnet exhibiting spontaneous magnetization below a Curie temperature (T_C) of 200 K (see Figure 5). The value of T_C was deduced from the intersection of a linear fit to the steepest part of the magnetization curve with the temperature axis at low applied fields.[26] Field-dependent measurements of μ_a versus T below 10 K showed a small, broad maximum near 4 K at low applied fields ($B_0 \leq 0.1$ T) only, suggesting the possibility of another magnetic transition. The origin of this broad maximum has not been explained; neutron diffraction experiments at temperatures below 10 K are needed in order to clarify this anomaly. Therefore, ferromagnetic order exists over the temperature range from 10 to 200 K. The paramagnetic region follows Curie–Weiss behavior only for $T > 350$ K (see Figure 6), with a Weiss constant (θ) of approximately +290 K, indicating strong Fe−Fe ferromagnetic exchange interactions. Nevertheless, further measurements at temperatures above 400 K are needed to fully confirm the Curie–Weiss behavior.

Ferromagnetic order is also indicated by the COHP analysis of the Fe−Fe interactions within the $Ti_9Fe_2Ru_{18}B_8$ structure: the antibonding Fe−Fe interactions observed at the Fermi level point toward a potential instability of the system with respect to spin polarization. Given a sufficient exchange splitting, redistribution of the electron spins to establish a net magnetization for the system may annihilate

(24) Dronskowski, R. *Computational Chemistry of Solid State Materials*; Wiley-VCH: Weinheim, Germany, 2005.

(25) Hatscher, S. T.; Schilder, H.; Lueken, H.; Urland, W. *Pure Appl. Chem.* **2005**, *77*, 497.

(26) Andrés, R.; Brissard, M.; Gruselle, M.; Train, C.; Vaissermann, J.; Malézieux, B.; Jamet, J.-P.; Verdaguer, M. *Inorg. Chem.* **2001**, *40*, 4633.

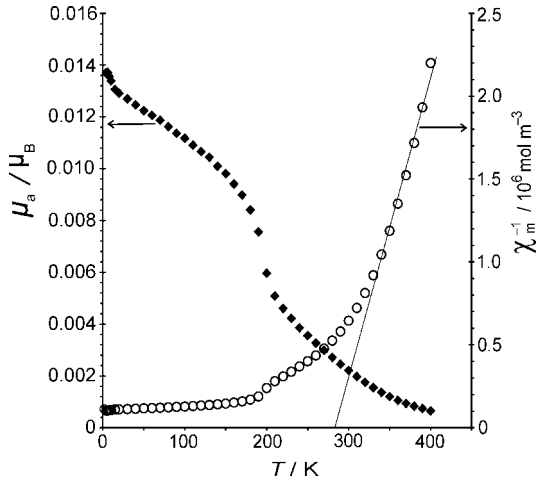

Figure 6. Magnetization (◆) and reciprocal susceptibility (○) as functions of temperature at an applied field of 0.01 T for $Ti_9Fe_2Ru_{18}B_8$. The solid line is a guide for the eyes.

antibonding interactions and lower the total energy.[24,27,28] This effect was seen in the present case, as the antibonding interactions at the Fermi level observed in the COHP curve for nonmagnetic Fe−Fe (see Figure 4b) disappeared when splitting into majority and minority spin bands occurred upon spin polarization (see Figure 4c). Our calculations also showed that the greatest contribution to the net magnetization from the Fe sites was a local magnetic moment of $2.45\mu_B$in which the centers of the Fe 3d majority and minority spin bands were split by 2.2 eV. There was a slight contribution from the Ru1 sites (magnetic moment of $0.18\mu_B$ and a 4d splitting of just 0.12 eV), while the remaining sites made negligible local contributions to the total magnetization. The calculated saturation moment for this system was therefore $5.1\mu_B$. However, the saturation moment could not be obtained experimentally because the system was far from saturation at 5 K and 7 T.

As a final observation, we note that ferromagnetic coupling between the Fe atoms in the Fe_2 dumbbell with such a short Fe−Fe distance may seem surprising. However, the site symmetry of this dimer in the crystal is D_{2h} (*mmm*). A molecular orbital (MO) analysis of an Fe_2 dimer having this site symmetry suggests that the ferromagnetic coupling within the dumbbell could be the result of Hund's rule for a half-filled, nearly degenerate pair of Fe−Fe π^* MOs. Figure 7 illustrates the results of MO calculations on a neutral Fe_2 dimer (in the intermetallic compound, there is very little net charge transfer; only a redistribution of orbital occupations occurs). In the gas-phase Fe_2 molecule (point group $D_{\infty h}$), the highest occupied MOs are the half-filled, doubly degenerate π^* orbitals. In the crystal under D_{2h} site symmetry, all of the degeneracies are strictly broken, and hybridization can occur within the Fe−Fe σ and δ bonding and antibonding orbitals but not with the π bonding and antibonding orbitals. Therefore, the π^* orbitals remain nearly degenerate and half-

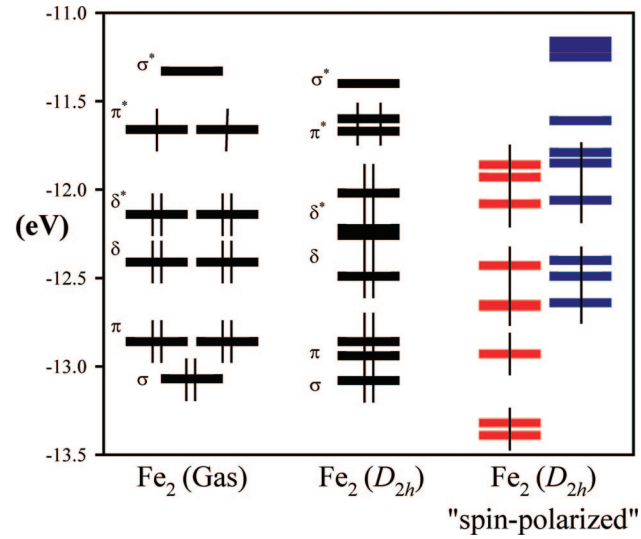

Figure 7. Molecular orbital diagrams for (left) gas-phase Fe_2 ($D_{\infty h}$ symmetry), (middle) Fe_2 under the D_{2h} symmetry of the dimer site in the $Ti_9Fe_2Ru_{18}B_8$ crystal, and (right) Fe_2 under D_{2h} symmetry with spin polarization applied. Occupied levels are indicated with vertical bars.

filled. According to Hund's rule, the most stable electronic configuration in this case is a spin triplet. Therefore, another interpretation that may contribute to understanding the observed ferromagnetism in $Ti_9Fe_2Ru_{18}B_8$ considers the Fe_2 dumbbells to be ferromagnetically coupled Fe_2 spin-triplet dimers. Ferromagnetic coupling along the *c* axis arises from spin polarization of the conduction bands because these Fe−Fe orbital interactions are strongly antibonding at the Fermi level in the nonmagnetic case. Ferromagnetic coupling within the Fe_2 dimer arises from the presence of a half-filled, nearly degenerate pair of orbitals. Further theoretical work is underway to assess the general nature of this model.

The occurrence of ferromagnetism in a boride containing mainly ruthenium atoms is new in the family of transition-metal borides. In fact, the majority of borides containing mostly ruthenium that have been synthesized and characterized to date (e.g., $Sc_2FeRu_5B_2$ and $Sc_2MnRu_5B_2$) are antiferromagnets,[6b] in contrast to those containing mainly rhodium, which are more likely to be ferromagnets than antiferromagnets.[5,6] These observations have been classified in terms of valence electron (VE) dependence in the case of $Ti_3Co_5B_2$-type compounds, which are antiferromagnets when the VE number is 62 or less and ferromagnets when the VE number is 65 or greater.[7] This trend has been correctly reproduced in the recently characterized $Sc_2FeRu_{5-n}Rh_nB_2$ series (in which the VE number varies from 60 to 65).[8a] Also, exchange interactions in this series have been studied using ab initio density functional calculations of the ground-state magnetic ordering,[8b] which revealed that significant Rh−Fe interactions were the leading contributors to ferromagnetic coupling in the rhodium-rich phases ($n > 2$) but that this was clearly not the case in the ruthenium-rich phases. Therefore, the unexpected presence of ferromagnetism in $Ti_9Fe_2Ru_{18}B_8$ may be attributed solely to the novel Fe_2 ladder structure found in this compound.

(27) (a) Landrum, G. A.; Dronskowski, R. *Angew. Chem.* **1999**, *111*, 1481. (b) Landrum, G. A.; Dronskowski, R. *Angew. Chem., Int. Ed.* **1999**, *38*, 1389.
(28) (a) Landrum, G. A.; Dronskowski, R. *Angew. Chem.* **2000**, *112*, 1598. (b) Landrum, G. A.; Dronskowski, R. *Angew. Chem., Int. Ed.* **2000**, *39*, 1560.

Conclusions

We have successfully synthesized the new compound $Ti_9Fe_2Ru_{18}B_8$, which is the first quaternary compound in the Ti−Fe−Ru−B system, and characterized it using single-crystal X-ray analysis and EDX measurements. $Ti_9Fe_2Ru_{18}B_8$ crystallizes as substitutional variant of the $Zn_{11}Rh_{18}B_8$-type structure and accommodates a ladder substructure composed of a magnetically active element (iron), observed here for the first time in an intermetallic compound. According to its electronic structure, the compound is metallic and predicted to be ferromagnetic. COHP bonding analysis indicated that Ru−B and Ti−Ru contacts are responsible for the structural robustness while Fe−Fe interactions influence the magnetic behavior. Magnetization measurements showed that $Ti_9Fe_2Ru_{18}B_8$ does indeed order ferromagnetically between 10 and 200 K. Finally, a model for ferromagnetism in this ladder-based structure identified ferromagnetic coupling among neighboring spin-triplet Fe_2 dimers along the *c* axis as the source of the magnetic behavior.

Acknowledgment. The authors acknowledge the generous financial support provided by a joint grant from the Deutsche Forschungsgemeinschaft (Germany) and the National Science Foundation (NSF DMR 05-02671) through the Materials World Network program as well as Resi Zaunbrecher (IPC, RWTH-Aachen) for the EDX analyses.

Supporting Information Available: Crystallographic information file for $Ti_9Fe_2Ru_{18}B_8$. This material is available free of charge via the Internet at http://pubs.acs.org.

IC7020963